Simulation of shock-induced instability using an essentially conservative adaptive CE/SE method*

Fu Zheng(付 峥)[a], Liu Kai-Xin(刘凯欣)[a)b)†], and Luo Ning(罗 宁)[a)b)c)‡]

[a] *LTCS and Department of Mechanics & Aerospace Engineering, College of Engineering, Peking University, Beijing* 100871, *China*
[b] *Center for Applied Physics and Technology, Peking University, Beijing* 100871, *China*
[c] *State Key Laboratory of Explosion Science and Technology, Beijing Institute of Technology, Beijing* 100081, *China*

(Received 29 April 2013; revised manuscript received 27 May 2013; published online 10 December 2013)

An essentially conservative adaptive space time conservation element and solution element (CE/SE) method is proposed for the effective simulation of shock-induced instability with low computational cost. Its implementation is based on redefined conservation elements (CEs) and solution elements (SEs), optimized interpolations and a Courant number insensitive CE/SE scheme. This approach is used in two applications, the Woodward double Mach reflection and a two-component Richtmyer–Meshkov instability experiment. This scheme reveals the essential features of the investigated cases, captures small unstable structures, and yields a solution that is consistent with the results from experiments or other high order methods.

Keywords: CE/SE method, shock-induced instability, adaptive mesh refinement

PACS: 02.60.Cb, 47.11.–j, 47.40.Nm, 47.20.Cq **DOI:** 10.1088/1674-1056/23/2/020202

1. Introduction

Shock-induced instability[1,2] (SII) is an active research subject because of its practical importance in areas of modern scientific research, including inertial confinement fusion (ICF),[3] deflagration-to-detonation transition (DDT),[4] and supernova explosions.[5] Such an instability often leads to material mixing and an eventual transition to turbulence at later stages. In ICF, the induced mixing of the capsule material and gaseous deuterium–tritium reduces the ability to efficiently ignite the fuel mixture. Meanwhile, in supersonic combustion, the mixing of fuel and air is essential for effective combustion and plays an important role in DDT. During the past few years, this has been intensively studied experimentally,[6] theoretically,[7] and numerically.[8] Experimental and theoretical studies of such phenomena remain challenging after decades of development. Numerical simulations can provide helpful information to understand the underlying physics. However, shock-accelerated instability poses computational challenges because of the extraordinary growth of the physical perturbation, the interaction between discontinuities (shocks, interfaces, and contacts), the possible presence of material mixing, and small scale vortices. Although traditional high-order schemes offer satisfying solutions, the required computational cost is generally expensive, especially of multi-dimensional problems. Moreover, shock-capturing schemes rely on numerical dissipation to stabilize the solution, while such an artificial diffusion must be prevented in order to describe the turbulent mixing accurately.[8]

To address these difficulties, we employ an explicit numerical framework to solve hyperbolic conservation laws, the CE/SE method.[9] Its unique and attractive features for solving SII problem include very little dissipation, local and global flux conservation in space and time, a novel shock capturing strategy without Riemann solvers, compact computational stencils, and the simultaneous calculation of variables and their spatial derivatives. The numerical tests by Wang *et al.*[10] have revealed that the CE/SE method with first-order derivatives is comparable to a fourth order essentially non-oscillatory scheme. Due to these advantages, this method has been successfully used in detonation,[11–13] multi-material elastic–plastic flows,[14] and spall fracture.[15,16]

In multi-dimensional applications, the CE/SE method has a number of limitations due to the extra computer resources required for calculating the spatial derivatives. The high computational cost can be effectively reduced with adaptive mesh refinement (AMR) methods. So far, only Jiang *et al.*[17] have presented an AMR–CE/SE method for solving magneto-hydrodynamic equations using the AMR package PARAMESH. Their approach slightly deviates from the conservation law due to the inappropriate interpolations of variables and derivatives. Thus, it may generate unphysical oscillation near strong shocks. In this work, an essentially conservative adaptive CE/SE (ECA–CE/SE) scheme with less computational cost and conservative error is established as a consistent extension of a variant high resolution unstructured

*Project supported by the National Natural Science Foundation of China (Grant Nos. 10732010, 10972010, and 11028206) and the Opening Project of State Key Laboratory of Explosion Science and Technology, China (Grant No. KFJJ13-5M).

†Corresponding author. E-mail: kliu@pku.edu.cn
‡Corresponding author. E-mail: ningl@pku.edu.cn

© 2014 Chinese Physical Society and IOP Publishing Ltd

CE/SE scheme.[18] The redefined conservation elements (CEs) and solution elements (SEs), and optimized interpolations are essential parts of our implementation. In the following paragraphs, we will give a detailed description of the ECA–CE/SE scheme.

2. Essentially conservative adaptive CE/SE method

Consider the following governing equations for two two-dimensional component flows:

$$\frac{\partial \boldsymbol{U}}{\partial t}+\frac{\partial \boldsymbol{E}}{\partial x}+\frac{\partial \boldsymbol{F}}{\partial y}=0, \tag{1}$$

where

$$\boldsymbol{U}=\begin{pmatrix}\rho\\ \rho u\\ \rho v\\ E\\ \rho Y\end{pmatrix},\quad \boldsymbol{E}=\begin{pmatrix}\rho u\\ \rho u^2+p\\ \rho uv\\ u(E+p)\\ u\rho Y\end{pmatrix},\quad \boldsymbol{F}=\begin{pmatrix}\rho v\\ \rho uv\\ \rho v^2+p\\ v(E+p)\\ v\rho Y\end{pmatrix},$$

and $E=p/(\gamma-1)+0.5\rho(u^2+v^2)$ with ρ, (u, v), E, Y, γ, and p denoting the density, velocity vector, total energy, mass fraction of the lighter gas, ratio of specific heat and pressure, respectively.

Firstly, we redefine CEs and SEs. Figure 1 illustrates the spatial topology of redefined CEs and SEs. P_i $(i=1, 2, 3, 4)$ and N_i $(i=1, 2, 3)$ denote centroids of original coarse grid cells and inserted grid cells, respectively. O_i $(i=1, 2, \ldots, 9)$ and M_i $(i=1, 2, \ldots, 6)$ represent centers of the original coarse grid edges and the inserted grid edges, respectively. Points A, B, C, D, E, F, G, and H are the original coarse grid nodes. Points with rectangular markers are the solution points (SPs) where the variables and derivatives are stored. Black color marks SPs at time level $t_n+0.5\mathrm{d}t$ and white color marks SPs at t_n or $t_n+\mathrm{d}t$ with the time step $\mathrm{d}t$. For SPs associated with CEs of the same size (e.g. P_1, N_1, and P_3), the ECA scheme is the structured scheme.[11] For the other SPs, the spatial computational domain is re-combined with smaller geometries. For example, the spatial domain for P_2 is divided into quadrilateral $EO_7P_2M_3$, $O_7BO_{10}P_2$, $P_2O_{10}CO_8$, $P_2O_8DM_4$, and triangle $M_3P_2M_4$. The novel domain for E consists of four quadrilaterals, $EO_6P_1O_7$, $EO_7P_2M_3$, $EM_3N_1M_2$, and $EM_2P_4O_6$. Integrations are also correspondingly modified using information from smaller grid cells. For example, the integration of a variable V over line DE becomes

$$\int_{DE}V\,\mathrm{d}l=\int_{DM_4}V\,\mathrm{d}l+\int_{M_4O_1}V\,\mathrm{d}l+\int_{O_1M_3}V\,\mathrm{d}l+\int_{M_3E}V\,\mathrm{d}l, \tag{2}$$

and the integration over rectangle DEO_7O_8 yields

$$\int_{DEO_7O_8}V\,\mathrm{d}s=\int_{EO_7P_2M_3}V\,\mathrm{d}s+\int_{M_3P_2M_4}V\,\mathrm{d}s+\int_{P_2O_8DM_4}V\,\mathrm{d}s. \tag{3}$$

According to Ref. [18], our redefinition eliminates conservative errors by different cell sizes. During the simulation, the time step is the same for all SPs. As is known, the CE/SE method is sensitive to short time step. Thus, spatial derivatives are calculated based on the Courant number insensitive CE/SE scheme.[19]

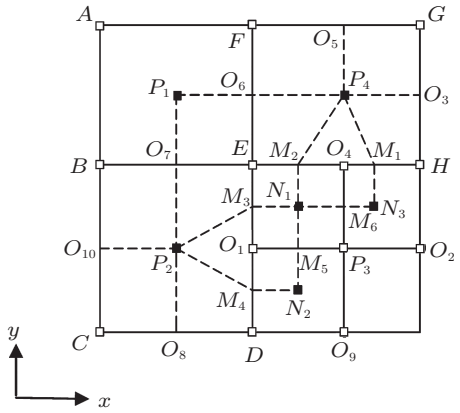


Fig. 1. Spatial geometries of CEs and SEs at neighboring levels of grid cells with original coarse mesh points A, B, C, D, E, F, G, H, and inserted mesh points O_1, O_2, O_4, O_9, and P_3.

The appropriate interpolation of variables and derivatives is another key part of the ECA–CE/SE scheme. We carefully compare five possible interpolations for variables and two for derivatives using the two-dimensional Sod shock tube problem in a unit square. Let V_1, V_2, $\mathrm{d}V_1$, and $\mathrm{d}V_2$ denote a variable and its derivative at the two ends of a line segment with a length of h. The inserted variable V_0 can be written as (i) $0.5(V_1+V_2)$ (average in Fig. 2), (ii) $0.5(V_1+V_2+0.25h(\mathrm{d}V_1+\mathrm{d}V_2))$ (Hermit in Fig. 2), (iii) $0.5(V_1+V_2+0.5h(\mathrm{d}V_1+\mathrm{d}V_2))$ (Taylor_aver in Fig. 2), (iv) $(V_1(|\mathrm{d}V_2|+\varepsilon)+V_2(|\mathrm{d}V_1|+\varepsilon))/(|\mathrm{d}V_1|+|\mathrm{d}V_2|+2\varepsilon)$ (CESE_aver in Fig. 2), or (v) $((V_1+0.5h\mathrm{d}V_1)(|\mathrm{d}V_2|+\varepsilon)+(V_2+0.5h\mathrm{d}V_2)(|\mathrm{d}V_1|+\varepsilon))/(|\mathrm{d}V_1|+|\mathrm{d}V_2|+2\varepsilon)$ (Taylor_CESE_aver in Fig. 2). The inserted derivative $\mathrm{d}V_0$ can be written as i) $(\mathrm{d}V_1|\mathrm{d}V_2|+\mathrm{d}V_2|\mathrm{d}V_1|)/(|\mathrm{d}V_1|+|\mathrm{d}V_2|+\varepsilon)$ (CESE_Daver in Fig. 3) or ii) $((V_0-V_1)|V_2-V_0|+(V_2-V_0)|V_1-V_0|))/(0.5h(|V_2-V_0|+|V_1-V_0|+\varepsilon))$ (CESE_Dcalc in Fig. 3). The constant number ε is 1×10^{-6}. Figures 2 and 3 compare the density distributions at $y=0.9$ by different interpolations. As illustrated in Figs. 2 and 3, interpolations (iv) and (i) capture sharper shocks but no excessive non-physical oscillations. Hence, they are introduced into the ECA–CE/SE scheme in the following simulations.

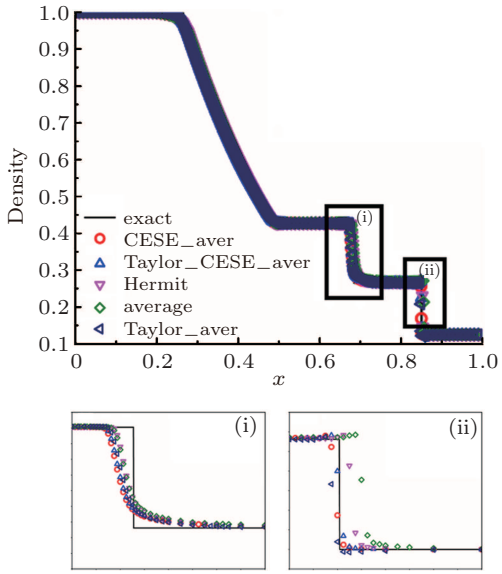


Fig. 2. (color online) Comparison among different interpolations for variables.

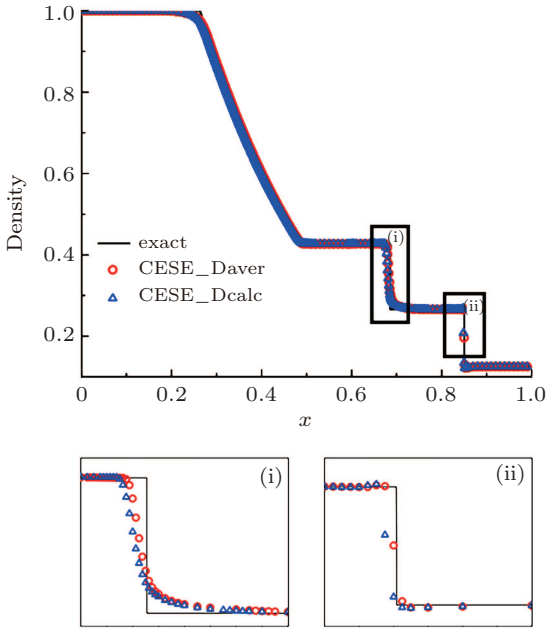


Fig. 3. (color online) Comparison among different interpolations for derivatives.

3. Numerical simulations

The ECA scheme is validated by an adiabatic blast problem with the sizes of grid cell ranging from 8^{-1} to 256^{-1}. In this problem, a blast wave is initialized from a high pressured circular region in the center of a unit square with the same parameters as those in Ref. [20]. In Fig. 4, the pressure distribution along the line $y = x$ at $t = 0.2$ by the ECA scheme (AMR-L6) is compared with the solution by the structured CE/SE method on a uniform 256^2 grid (CESE-256). The results are consistent with those in Ref. [20], and they demonstrate the good symmetry and high resolution of discontinuities, which confirm the ECA–CE/SE scheme for the following more difficult applications.

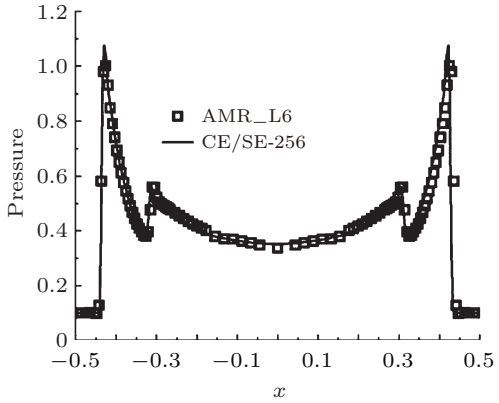


Fig. 4. Comparison between the ECA scheme and the structured scheme.

The double Mach reflection problem[21] is calculated to demonstrate the capability of the ECA scheme for the capture of instability structures in single component flows. A shock of Mach 10 at a 60° angle with respect to the x axis is initially set up at $x = 1/6$, $y = 0$ in a rectangle $[0, 4]\times[0, 1]$. The shock is reflected from the bottom wall and propagates rapidly toward the right end. Double Mach reflection with two Mach stems and two contact discontinuities is observed and a wall–jet forms near the wall below the contact discontinuity within $[2.1, 2.8]\times[0, 0.5]$. The exhibited physical instability (the rolling up and vortices) will increase with higher resolution due to the non-dissipative Euler equations. It is generally accepted that the prediction of such instabilities is a measure of resolution of a scheme for the Euler equations. Thus, it has been extensively used to evaluate high order schemes.[22]

In this problem, the size of the grid cell is between 10^{-1} and 1280^{-1} with total grid levels 8. The density contours at $t = 0.2$ are shown in Fig. 5. The ECA–CE/SE scheme predicts the wavy contact discontinuities and the clear vortex structure near the wall at $x = 2.65$. The performance is qualitatively comparable to that from a fifth order WENO method (it is third order accurate at shocks) on a uniform grid corresponding to the smallest cells. The cost memory is less than 10% of the corresponding structured scheme and 40% of the WENO scheme, showing the potential of nine time large scale simulations. The computational time is reduced to approximately 10% of the corresponding structure scheme or 5% of the WENO scheme. This efficiency is equivalent to a parallel CE/SE approach on 12 CPUs. The above results indicate that the ECA–CE/SE scheme is suitable for effective simulation of shock-induced strong instability in single component flows.

The next application is a two-component single mode Richtmyer–Meshkov instability (RMI) case[8,23,24] with an incident shock of Mach 1.21 and re-shock at approximately 6.1 ms. Induced by the deposition of the baroclinic vorticity term ($\nabla\rho \times \nabla p$), the initial perturbed interface grows linearly and then evolves into nonlinear structures with spikes and bubbles, and eventually evolves into turbulent mixing. In

the present computation, the parameters in Ref. [24] are used to match the experiment. The initial air–acetone/SF_6 interface is perturbed in the manner of $\eta(x) = a_0 \sin(kx)$ with amplitude a_0 2 mm and wavelength $2\pi/k$ 5.93 cm. The interfacial diffusion of width 5 mm is described with the function in Ref. [8]. Outflow boundary conditions are set up at the entrance of the shock tube, and reflecting boundary conditions are used at the other walls. The above boundary conditions avoid the driver-based expansion wave, leading to a more accurate exhibition of the true nature of the RMI.

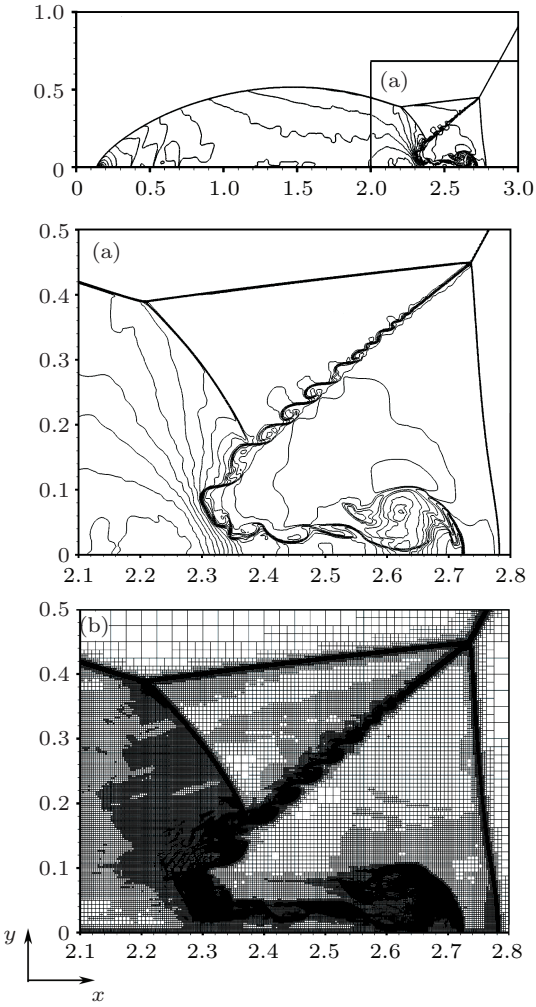


Fig. 5. Density distributions of the double Mach reflection test by the ECA–CE/SE scheme with 25 equally spaced contour lines from 2 to 22. (a) Details within [2.1, 2.8]×[0, 0.5], (b) grid distribution inside [2.1, 2.8]×[0, 0.5] with grid cell levels 3∼8.

In Fig. 6, the numerical history of density on a grid with maximal 512 cells per wave-length is compared with the experimental data at 3, 4, 5, 6, 7, and 7.8 ms. The cell size is particularly selected to avoid the production of unphysical small-scale features. During RMI simulations, inappropriate approximation of the multiple specific heat ratios across the interface causes pressure oscillations and further contaminates the entire physical field. To avoid the contamination, Latini *et al.*[24] used a single value of the specific heat ratio 1.276, corresponding to the air–acetone mixture. Their results show that the selected single value is sufficient for simulating the experiment in Ref. [23]. Hence, the same strategy is employed in this work.

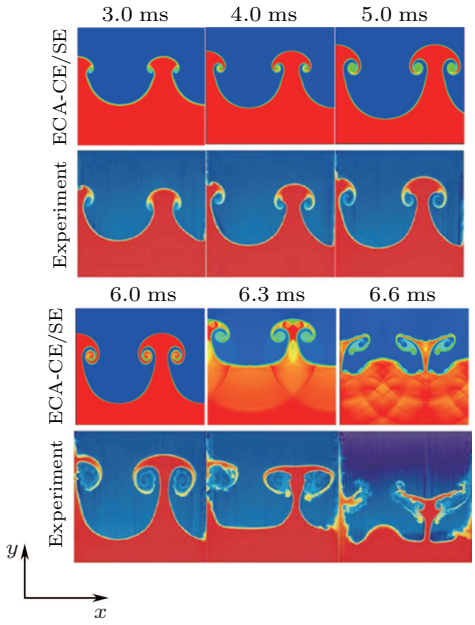


Fig. 6. (color online) Comparisons of the ECA–CE/SE simulation with the experimental data at 3, 4, 5, 6, 7, and 7.8 ms. The two gases are air–acetone (top) and SF_6 (bottom).

In general, the numerical results and experimental images are in good agreement. The penetration of spikes into air–acetone and bubbles into SF_6, and the roll-up structures in the vortex core are well represented by the ECA–CE/SE simulation. Small differences are observed at the "cap" of the mushroom shape. The computed roll-up structures are more compact. The sequence of numerical images is also earlier, by approximately 1.2 ms. These are the direct consequence of the absence of the driver-based expansion wave, which decelerates the contact interface and expands the mixing layer. The rarefaction also causes the formation of small-scale structures on the interface. After re-shock, numerical images capture essential features of the RMI experiment. The reflected shock directly collides with the travelling interface and re-distributes vortices. Suddenly, bubbles and spikes change directions and travel toward each other, resulting in a reduction of the penetration. Eventually, bubbles and spikes are inverted and they grow in opposite directions. The redistributed vortices are responsible for the transition between spikes and bubbles. Enhanced by the Kelvin–Helmholtz instability, they also induce novel small unstable structures at the "root" of the mushroom at 6.6 ms in Fig. 6.

Another great interest in RMI investigations[24,25] is to predict the bubble and spike locations (denoted as x_b and x_s, respectively) and the resulting amplitude of the mixing layer $a_m = (x_s - x_b)/2$. We compare the computed amplitude with corresponding experimental data[23] in Fig. 7. The ECA–CE/SE scheme gives a consistent solution with experimental

results without re-shock. Referring to Fig. 7, there is a sudden drop at 6.125 ms and a rise-up at 6.4 ms. Before the shock reaches spikes, the bubbles change directions, chase spikes and initiate the drop. Then, the bubbles and spikes begin to be converted into each other. As a result, the "root" of spikes turns into new "bubbles" and the side "edge" of the mushroom "cap" becomes new "spikes" as shown in Fig. 6. Since new "spikes" travel faster than new "bubbles", the amplitude grows and the rise-up begins.

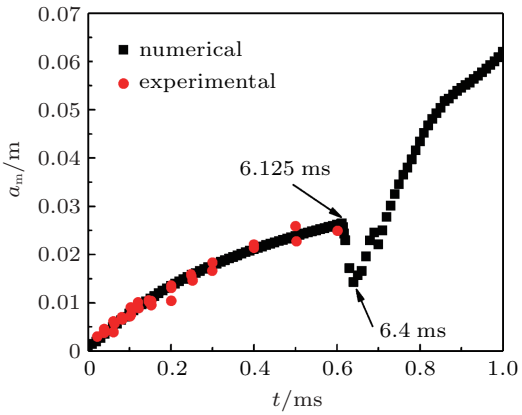


Fig. 7. (color online) Comparison between experimental and numerical amplitude of mixing layer a_m.

4. Conclusion

In this paper, an ECA–CE/SE method is built for the simulation of SII with low cost. In our AMR implementation, non-conservation due to different neighboring cell sizes is eliminated by an extension of CEs and SEs in Ref. [18]. High discontinuity resolution is also obtained using optimized interpolations. The ECA–CE/SE scheme is used to numerically simulate two SII cases, the Woodward double Mach reflection and a two-component RMI experiment. The numerical results are consistent with the RMI experimental results or other numerical investigations. Furthermore, the detailed essential characteristics, including small vortices along discontinuities and roll-up structures in both cases and the evolution of the amplitude of mixing layer in RMI, are clearly revealed by the ECA–CE/SE scheme.

References

[1] Richtmyer R D 1960 *Commun. Pure Appl. Math.* **13** 297
[2] Meshkov E E 1969 *Fluid Dyn.* **4** 101
[3] Nakai S and Takabe H 1996 *Rep. Prog. Phys.* **59** 1071
[4] Yasunaga K, Mikajiri T, Sarathy S M, Koike T, Gillespie F, Nagy T, Simmie J M and Curran H J 2012 *Combust. Flame.* **159** 2138
[5] Arnett D 2000 *Astrophys. J. Suppl. Ser.* **127** 213
[6] Long C C, Krivets V V and Jacobs J W 2009 *Phys. Fluids* **21** 114104
[7] Mikaelian K O 2011 *Physica D* **240** 935
[8] Movahed P and Johnsen E 2013 *J. Comput. Phys.* **239** 166
[9] Chang S C 1995 *J. Comput. Phys.* **119** 295
[10] Wang X Y, Chang S C and Jorgenson P C E 2000 *AIAA* 2000-0474
[11] Wang G, Zhang D L and Liu K X 2007 *Chin. Phys. Lett.* **24** 3563
[12] Wang G, Zhang D L and Liu K X 2010 *Chin. Phys. Lett.* **27** 024701
[13] Wang G, Zhang D L and Liu K X 2011 *Comput. Phys. Commun.* **182** 1589
[14] Wang J T, Liu K X and Zhang D L 2009 *Comput. Fluids* **38** 544
[15] Chen Q Y, Chen Q Y, Wang J T and Liu K X 2010 *J. Comput. Phys.* **229** 7503
[16] Chen Q Y and Liu K X 2011 *Chin. Phys. Lett.* **28** 06460
[17] Jiang C W, Cui S X and Feng X S 2012 *Comput. Fluids* **54** 105
[18] Fu Z and Liu K X 2012 *Chin. Phys. B* **21** 040202
[19] Chang S C 2002 *AIAA* 2002-3890
[20] Skinner M A and Ostriker E C 2010 *Astrophys. J. Suppl. Ser.* **188** 290
[21] Woodward P and Colella P 1984 *J. Comput. Phys.* **54** 115
[22] Shi J, Zhang Y T and Shu C W 2003 *J. Comput. Phys.* **186** 690
[23] Collins B D and Jacobs J W 2002 *J. Fluid Mech.* **464** 113
[24] Latini M, Schilling O and Don W S 2007 *Phys. Fluids* **19** 024104
[25] Ukai S, Balakrishnan K and Menon S 2011 *Shock Waves* **21** 533